EFFECT OF FIXING ABSOLUTE MAGNITUDE OF TYPE Ia SUPERNOVAE ON THE HUBBLE TENSION

PROJECT REPORT

Submitted by

SARAH S PANIKULANGARA

Register No.: AM23PHY009

Under the guidance of

Dr. MINU PIUS

Assistant Professor

Department of Physics

St. Teresa's College (Autonomous), Ernakulam

Kochi – 682011

Submitted to

Mahatma Gandhi University, Kottayam

In partial fulfillment of the requirements for the award of the degree of

MASTER OF SCIENCE IN PHYSICS

DEPARTMENT OF PHYSICS

ST. TERESA'S COLLEGE (AUTONOMOUS), ERNAKULAM

DEPARTMENT OF PHYSICS
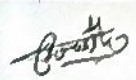## ST. TERESA'S COLLEGE (AUTONOMOUS), ERNAKULAM

CERTIFICATE

This is to certify that the project report entitled " **EFFECT OF FIXING ABSOLUTE MAGNITUDE OF TYPE Ia SUPERNOVAE ON THE HUBBLE TENSION**" is an authentic work done by **SARAH S PANIKULANGARA (AM23PHY009)** under my guidance at the Department of Physics, St. Teresa's College (Autonomous), Ernakulam for the partial fulfillment of the requirements for the award of the Degree of Master of Science in Physics during the year 2024–25. The work presented in this dissertation has not been submitted for any other degree in this or any other university.

Supervising Guide

Dr. MINU PIUS

External Guide

Dr. SARATH NELLERI

Post Doctoral Fellow

Indian Institute of Technology, Kanpur

Head of the Department

Dr. MARY VINAYA

Place: Ernakulam

Date: 3/5/2025

DEPARTMENT OF PHYSICS
ST. TERESA'S COLLEGE (AUTONOMOUS), ERNAKULAM

M.Sc. PHYSICS

PROJECT REPORT

Name : Sarah S Panikulangara

Register No. : AM23PHY009

Year of Work : 2024–2025

This is to certify that the project entitled "EFFECT OF FIXING ABSOLUTE MAGNITUDE OF TYPE Ia SUPERNOVAE ON THE HUBBLE TENSION" is an authentic work done by **Sarah S Panikulangara**

Staff Member In-charge

Dr. Minu Pius

Assistant Professor

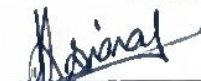**Head of the Department**

Dr. Mary Vinaya

Assistant Professor

Submitted for the university examination held at St. Teresa's College (Autonomous), Ernakulam.

Date: 3|5|25

Examiners:

DECLARATION

I, **SARAH S PANIKULANGARA**, final year M.Sc. Physics student of the Department of Physics and Centre for Research, St. Teresa's College (Autonomous), Ernakulam, do hereby declare that the project report entitled **"EFFECT OF FIXING ABSOLUTE MAGNITUDE OF TYPE Ia SUPERNOVAE ON THE HUBBLE TENSION"** has been originally carried out under the guidance and supervision of **Dr. MINU PIUS**, Assistant Professor, Department of Physics, St. Teresa's College (Autonomous), Ernakulam in partial fulfilment for the award of the Degree of Master of Physics. I further declare that this project is not partially or wholly submitted for any other purpose and the data included in this project is collected from various sources and are true to the best of my knowledge.

PLACE: Ernakulam

DATE: 3/5/2025

Ms. Sarah S Panikulangara

<u>ACKNOWLEDGMENT</u>

I would also like to express my heartfelt thanks to my friends Mr. Sreeragh Radakrishnan, Ms. Angeline Anna Varghees and Ms. Beaula Maria Thomas for their unwavering support and help throughout my project. Their encouragement, thoughtful advice, and constant presence made a significant difference in completing this work.
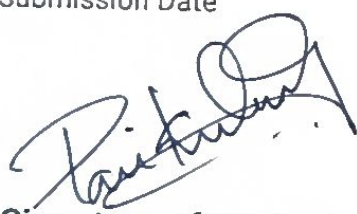
I am grateful to all my family members for their encouragement and support, which played a vital role in helping me complete this work. Lastly, I wish to thank everyone who contributed, directly or indirectly, to the successful completion of this thesis.

List of Tables

List of Figures

Contents

Chapter 1

Review of Observational Cosmology

1.1 Introduction

Cosmology is relatively a new branch of physical science. It deals with the origin, evolution, and ultimate fate of the universe. Humans have been observing the celestial bodies since ancient times. The invention of telescopes allowed us to observe the stars and other objects in greater detail. The development of a variety of instruments allowed us to investigate the universe in other regions of the electromagnetic spectrum. These observations were based on the Copernican principle which tells that the universe looks the same independent of the observer.

Modern cosmology is based on the assumption that the large scale (about 100 Mpc) universe possesses two important properties, homogeneity and isotropy of space. Homogeneity is the statement that the universe looks the same at each point and isotropy states that the universe looks the same in all directions. The modern era of scientific cosmology began with Einstein's general theory of relativity, published in 1916. According to Einstein's theory, the matter or energy changes the geometry of spacetime and any trajectory of an object in this spacetime is determined by the curvature of spacetime.

The fundamental equation in general relativity is the Einstein's gravitational field equation:

$$G_{\mu\nu} = \frac{8\pi G}{c^4} T_{\mu\nu}$$

1.2 Baryon Acoustic Oscillations (BAO)

Baryon Acoustic Oscillations (BAO) are fluctuations in the density of visible baryonic matter in the universe, arising from acoustic waves in the primordial plasma of tightly coupled photons and baryons during the early universe. These oscillations left a lasting imprint on the large-scale structure of the universe. As the universe cooled and the photons decoupled from the baryons, gravity began to dominate, pulling baryons together into shells with a fixed radius known as the sound horizon. The sound horizon, denoted by r_d, is given by the integral

$$r_d = \int_{z_d}^{\infty} \frac{c_s(z)}{H(z)} \, dz,$$

where $c_s(z)$ is the sound speed as a function of redshift z, and z_d is the redshift at which photons and baryons decoupled.

BAO provides a "standard ruler" for measuring cosmological distances. A standard ruler is an object whose absolute size is known, and by measuring its apparent size, one can determine its distance from the observer. The "standard ruler" for BAO is defined by the sound horizon at the epoch of recombination, corresponding to approximately 490 million light years in the modern universe. This scale is measurable by analyzing the large-scale structure of the universe, particularly the clustering of galaxies. The density fluctuations caused by BAO are visible in the two-point correlation function of galaxies or in the angular power spectrum of the Cosmic Microwave Background (CMB) anisotropies.

In addition to the CMB, BAO signals are detectable in the clustering of galaxies. Early redshift surveys, such as the Sloan Digital Sky Survey (SDSS)[1] and the 2-degree Field Galaxy Redshift Survey (2dFGRS), directly observed the BAO signature in 2005. These surveys revealed that the BAO signal in the modern universe corresponds to a length scale of about 150 Mpc. The temperature fluctuations in the CMB, which are related to the different densities of matter in the early universe, can be directly associated with BAO, providing an independent means of constraining cosmological parameters.[3, ?]

The BAO imprints in the CMB and the galaxy distribution are crucial for understanding

the expansion history of the universe. By comparing the BAO peaks in the CMB and galaxy surveys, we can derive important cosmological parameters such as the Hubble parameter $H(z)$ and the angular diameter distance $D_A(z)$. This method also allows for the study of dark energy, dark matter, and baryonic matter. Furthermore, the variation of BAO signatures over time provides an independent means of measuring the universe's expansion rate and constraining the evolution of cosmological components.

The detection of BAO and its evolution over time also helps in testing various cosmological models, particularly through the Alcock-Paczynski (AP) test, which provides an independent measurement of the angular diameter distance and the Hubble parameter. This makes BAO an essential tool in modern cosmology for refining our understanding of the universe's structure and expansion.

1.3   Type Ia Supernovae and Their Role in Cosmology

Type Ia supernovae (SNe Ia) are among the most significant astrophysical phenomena used in the study of cosmology. These powerful explosions occur in binary star systems where one component is a white dwarf composed of carbon and oxygen. When the white dwarf accretes matter from its companion star and its mass approaches the Chandrasekhar limit (approximately 1.44 solar masses), the internal pressure becomes sufficient to ignite runaway carbon fusion. This results in a thermonuclear explosion that completely disrupts the white dwarf.

One of the most remarkable properties of SNe Ia is their consistent peak luminosity. Since they explode at nearly the same critical mass, their intrinsic brightness remains relatively uniform, making them excellent *standard candles*. This allows astronomers to determine distances across the universe by comparing their absolute magnitude (M) with their observed apparent magnitude (m). The relationship is described by the distance modulus:

$$\mu = m - M = 5 \log_{10} \left(\frac{d_L}{\text{Mpc}} \right) + 25,$$

where d_L is the luminosity distance. This distance can be theoretically calculated for a given

redshift z using the cosmological parameters:

$$d_L = (1 + z) \int_0^z \frac{dz'}{H(z')}.$$

Type Ia supernovae are spectroscopically identified by a strong silicon (Si II) absorption line near 6150 Å. This feature distinguishes them from other Type I supernovae, such as Type Ib and Ic, which either show helium lines or lack both helium and silicon features. The uniformity in their light curves allows for further standardization by correlating the peak brightness with the light curve shape and color, improving the accuracy of distance estimates to about 6–8%.

The cosmological significance of SNe Ia was dramatically highlighted in 1998 when two independent research teams — the Supernova Cosmology Project and the High-Z Supernova Search Team — observed distant SNe Ia that appeared dimmer than expected. This observation implied that the universe's expansion was accelerating, a groundbreaking discovery that led to the introduction of the concept of *dark energy*. These findings provided the first direct evidence that the universe is not only expanding but doing so at an accelerating rate.

Additionally, observations of SNe Ia are central to measuring the current value of the Hubble constant (H_0). When used in conjunction with Cepheid variable stars, they yield highly precise local measurements of H_0. However, a notable discrepancy — known as the *Hubble tension* — exists between these locally determined values and those derived from cosmic microwave background (CMB) data under the ΛCDM model. This tension has become one of the most discussed challenges in contemporary cosmology, sparking investigations into possible new physics or hidden systematic errors in the data.

In summary, Type Ia supernovae serve as powerful tools in cosmology, enabling the determination of cosmic distances, supporting the discovery of the accelerating universe, and contributing significantly to our understanding of the universe's expansion history and composition.

1.4 Cosmic Microwave Background: Evidence and Observations

The Cosmic Microwave Background (CMB) is the residual thermal radiation from the Big Bang, providing a snapshot of the universe approximately 380,000 years after its inception. Initially predicted by Alpher and Gamow in 1948, the CMB was serendipitously detected in 1965 by Arno Penzias and Robert Wilson at Bell Labs, who observed an isotropic microwave signal of about 3 K, which they attributed to a uniform background radiation [6].

At early times, the universe was a hot, dense plasma of protons, electrons, and photons, preventing the formation of neutral atoms due to high photon energies. As the universe expanded and cooled, photons became less energetic, allowing atoms to form and the universe to become transparent. This epoch, known as the decoupling epoch, released photons with a blackbody spectrum at a temperature of approximately 3000 K. Over time, these photons have redshifted to the microwave region, now observed as the CMB with a temperature of about 2.7 K.

To accurately study the CMB, space-based observations are essential due to atmospheric interference at ground level. The Cosmic Background Explorer (COBE) satellite, launched in 1989, was the first to measure the CMB spectrum, confirming its near-perfect blackbody nature. COBE also detected temperature anisotropies, marking the first significant detection of CMB fluctuations [?].

Subsequent missions, such as the Wilkinson Microwave Anisotropy Probe (WMAP) launched in 2001, provided higher-resolution maps of the CMB, offering precise measurements of cosmological parameters like the density of ordinary matter, dark matter, and dark energy. The Planck satellite, launched by the European Space Agency in 2009, further refined these measurements, determining the effective number of neutrino species and providing tight constraints on the flatness of the universe [?].

The CMB's temperature anisotropies arise from inhomogeneities in the early universe, including baryonic acoustic oscillations. These anisotropies serve as a powerful probe for understanding the universe's composition and evolution, with the CMB angular power spectrum

allowing for the determination of cosmological parameters to percent-level accuracy.

In summary, the CMB serves as a critical observational tool in cosmology, providing insights into the universe's early conditions and supporting the Big Bang model of cosmology.

1.5   Observational Hubble Parameter Data

The Hubble parameter, $H(z)$, characterizes the expansion rate of the Universe as a function of redshift and is central to cosmological analysis. Although $H(z)$ is not directly observable, it can be inferred from observational quantities like cosmic chronometers (standard clocks) and Baryon Acoustic Oscillations (BAO) (standard rulers). One particularly effective method to derive $H(z)$ involves the differential ages of galaxies. By comparing the ages of passively evolving galaxies at different redshifts, the derivative $\frac{dz}{dt}$ can be computed, yielding $H(z)$ through the relation:

$$H(z) = -\frac{1}{1+z}\frac{dz}{dt}.$$

This technique, known as the cosmic chronometer approach, has been widely applied in recent years, allowing the estimation of $H(z)$ values across redshifts up to $z \sim 2.36$.[15, 8] These measurements depend on selecting suitable galaxy samples and applying stellar population synthesis models to estimate age differences reliably. Once the age differential is obtained, it becomes possible to track how the expansion rate varies over time.

Another key method uses the imprint of BAO in large-scale structures. These acoustic oscillations provide characteristic length scales that act as cosmic rulers. By measuring these features at various redshifts in galaxy distributions and the Lyα forest, additional $H(z)$ data points are generated.

An example of this practical use is the Hubble Space Telescope (HST), which uses observations of Cepheid variable stars to calibrate the distance-redshift relationship, and hence determine H_0, the Hubble constant. The recent estimate from local measurements stands at $H_0 = 73.48 \pm 1.66$ km s^{-1} Mpc^{-1}, derived via this method. This value is essential for determining the age and scale of the observable universe.

Under the ΛCDM model, the evolution of the Hubble parameter is given by:

$$H(z) = H_0\sqrt{\Omega_m(1+z)^3 + \Omega_\Lambda},$$

where Ω_m and Ω_Λ represent the matter and dark energy density parameters, respectively. This formula links the expansion rate to the matter content of the universe and its curvature.

Despite the utility of these methods, one challenge with $H(z)$ data is the limited number of reliable observations compared to other cosmological probes. Furthermore, at higher redshifts, the associated uncertainties tend to increase, which constrains precision. Nevertheless, the data provide an important tool for testing cosmological models, including those beyond the standard ΛCDM framework. They also play a crucial role in constraining the behavior and evolution of dark energy by probing its influence on the expansion history.

Overall, the compilation and analysis of observational Hubble parameter data offer insights into the dynamics of cosmic expansion and remain a vital part of modern cosmology.

1.6   Large Scale Structure

The Large Scale Structure (LSS) of the Universe refers to the large-scale distribution of galaxies, galaxy clusters, and other cosmic objects. This structure extends over vast distances, much larger than individual galaxies, and includes features such as galaxy clusters, voids, and filaments. These patterns are primarily shaped by gravitational forces, which pull matter together, creating dense regions and vast voids between them. The study of LSS provides essential insights into the evolution of the universe and the formation of cosmic structures.

LSS formation is deeply tied to the process of structure formation, which is responsible for the creation of galaxies and galaxy clusters from minute density fluctuations in the early universe. These fluctuations, initially present as quantum ripples, were magnified by cosmic inflation, leading to slight overdensities and underdensities in the early universe. As the universe expanded, radiation density decreased more rapidly than matter density, causing the dark matter fluctuations to grow, creating the seeds from which galaxies and clusters eventually

formed.

To map and study LSS, astronomers rely on large-scale galaxy surveys and redshift surveys. Prominent examples include the Sloan Digital Sky Survey (SDSS) and the Two-Degree Field Galaxy Redshift Survey (2dFGRS). These surveys have provided detailed maps of the large-scale galaxy distribution, revealing a sponge-like structure composed of filaments and vast voids. These surveys offer crucial data on the distribution of matter, dark energy, and the rate of cosmic expansion.

Through these galaxy surveys, it has been observed that galaxies are not uniformly distributed. Instead, the universe is made up of clusters of galaxies, which are over-dense regions, and voids, which are under-dense regions. These structures range from a few megaparsecs to tens of megaparsecs in size. The galaxy correlation function, a statistical tool that quantifies the distribution of galaxies, provides a means to measure the correlation properties of underlying dark matter. By analyzing this function, cosmologists can infer critical cosmological parameters, such as the matter density and the amplitude of density fluctuations from the early universe.

A particularly important feature observed in the galaxy correlation function is the presence of baryon acoustic oscillations (BAO). These oscillations, which were first detected by surveys like SDSS and 2dFGRS, appear as a "bump" in the correlation function. BAO are the result of sound waves propagating through the early universe's plasma, and their signature can be used to determine key cosmological parameters. By studying the shape and amplitude of the BAO feature, cosmologists can gain insight into the matter density and the rate of cosmic expansion, which in turn helps to constrain the properties of dark energy.

The anisotropies observed in the Cosmic Microwave Background (CMB) also provide valuable information about the formation of LSS. These early fluctuations in temperature are connected to the density fluctuations in the early universe that later grew into the structures we observe today. Thus, the study of the large-scale distribution of galaxies, coupled with the analysis of the CMB and galaxy correlation functions, allows cosmologists to probe the expansion history of the universe and test different cosmological models.

Overall, the study of LSS is crucial for understanding the evolution of the universe, the distribution of dark matter, and the role of dark energy in cosmic expansion. By analyzing galaxy surveys and redshift data, researchers can refine our understanding of how the universe grew from its early, homogeneous state to the complex, large-scale structure we observe today.[2]

1.7   Gravitational Waves

Gravitational waves are ripples in the fabric of spacetime caused by the acceleration of massive objects, such as merging black holes or neutron stars. These waves propagate at the speed of light and carry crucial information about their origins, including the nature of gravity and the events that caused them. First predicted by Albert Einstein in 1915 as a part of his general theory of relativity, the existence of gravitational waves was confirmed a century later with the direct detection of a signal named GW150914 on September 14, 2015, by the Laser Interferometer Gravitational-Wave Observatory (LIGO) collaboration. The waves were produced by the merger of two black holes approximately 1.3 billion light-years away. This marked a significant breakthrough in astrophysics, confirming a key prediction of general relativity and opening a new observational window to the universe.

Since the detection of the first gravitational wave signal, LIGO, together with the Virgo and KAGRA collaborations, has detected many more gravitational wave events. Notably, on August 14, 2017, the LIGO-Virgo network observed gravitational waves from a binary black hole merger, named GW170814, and a few days later, detected the merger of two neutron stars, dubbed GW170817. The latter event provided additional insights, as electromagnetic signals were also detected across various wavebands, allowing for the study of both gravitational waves and electromagnetic radiation from the same cosmic event. This simultaneous observation enabled scientists to determine the luminosity distance of the event directly from the gravitational waves, and the redshift from the electromagnetic counterpart, thus providing a means to calculate the velocity and Hubble constant.

Gravitational waves offer a powerful tool to explore the expansion history of the universe,

dark energy's role in this expansion, and the fundamental nature of spacetime. The direct detection of gravitational waves allows for the measurement of luminosity distances, which, when combined with the redshift information from electromagnetic signals, provide a means to calculate the velocity of the source. This, in turn, facilitates the determination of the Hubble constant, providing a new approach to measure the rate of expansion of the universe. Observing gravitational waves also allows for the study of cosmological parameters such as the density of matter and the contribution of dark energy to the universe's expansion.

Furthermore, primordial gravitational waves, which originated from the early universe during inflation, can offer valuable insights into the conditions that prevailed just after the Big Bang. These waves have been detected through pulsar timing arrays[10], and their study helps constrain inflationary models, specifically the scale of inflation and the slow-roll parameters that govern the early cosmic expansion.

In addition to expanding our understanding of cosmic events, gravitational waves are pivotal in testing the theoretical framework of general relativity. They provide direct evidence of the behavior of spacetime in extreme conditions and are essential tools for refining our understanding of the universe's evolution. Gravitational wave astronomy is thus a revolutionary step forward, enabling the study of phenomena that were previously unreachable by traditional electromagnetic observation methods, and offering profound insights into the fundamental forces and structures of the universe.

Chapter 2

ΛCDM - Standard Model of Cosmology

2.1 Introduction

The discovery of cosmic acceleration has led to the ΛCDM model becoming the standard cosmological model for the universe. The ΛCDM model is grounded in the principles of General Relativity and offers a comprehensive framework for understanding the composition and evolution of the universe. According to this model, the universe is primarily composed of three components: dark energy (DE), cold dark matter (CDM), and ordinary baryonic matter. Dark energy, in the form of the cosmological constant (Λ), accounts for approximately 72% of the universe's total energy. Cold dark matter contributes around 23%, while ordinary matter, including the baryonic matter that forms galaxies and other structures, makes up only about 4.6%.[4]

The ΛCDMCDM model successfully explains the observed acceleration of the universe's expansion. It also predicts the distribution of these energy components and their role in shaping the universe, as illustrated in Figure 2.1. Dark matter remains one of the most intriguing and elusive components of the universe. While its exact nature

2.2   Einstein's Gravitational Field Equations

The General Theory of Relativity, introduced by Albert Einstein in 1915, revolutionized our understanding of the cosmos by establishing a deep connection between the geometry of space-time and the distribution of matter and energy. At the core of this theory lie the gravitational field equations, which are a set of ten non-linear partial differential equations involving four independent variables. These equations describe how matter and energy influence the curvature of spacetime.[11]

The field equations are expressed as:

$$G_{\mu\nu} = \frac{8\pi G}{c^4} T_{\mu\nu} \tag{2.1}$$

Here, $G_{\mu\nu}$ is the Einstein tensor, which encapsulates the curvature of spacetime. It is defined in terms of the Ricci curvature tensor $R_{\mu\nu}$, the Ricci scalar R, and the metric tensor $g_{\mu\nu}$ as:

$$G_{\mu\nu} = R_{\mu\nu} - \frac{1}{2} R g_{\mu\nu} \tag{2.2}$$

The Ricci scalar R is the trace of the Ricci tensor, given by $R = g^{\mu\nu} R_{\mu\nu}$. The right-hand side of the equation features the energy-momentum tensor $T_{\mu\nu}$, a second-order tensor that represents the distribution and flow of energy and momentum in spacetime. For a perfect fluid, the energy-momentum tensor takes the form:

$$T_{\mu\nu} = (\rho + p)u_\mu u_\nu + p g_{\mu\nu} \tag{2.3}$$

where ρ is the energy density, p is the pressure, and u^μ is the four-velocity of the fluid.

Einstein's field equations demonstrate that the geometry of spacetime is shaped by the presence and movement of matter and energy. This relationship implies that the universe must be dynamic, either expanding or contracting. However, Einstein initially sought a static model of the universe and introduced the cosmological constant Λ, which contributes a repulsive effect counteracting gravitational attraction. This modified the field equations to:

$$R_{\mu\nu} - \frac{1}{2}Rg_{\mu\nu} + \Lambda g_{\mu\nu} = \frac{8\pi G}{c^4}T_{\mu\nu} \tag{2.4}$$

This form allows for a static solution under certain conditions. Nevertheless, observations by Edwin Hubble in the late 1920s revealed that the universe is expanding, prompting Einstein to retract the cosmological constant, though it later regained relevance in the context of dark energy.

These equations can also be derived from a variational principle using the Einstein-Hilbert action, which is given by:

$$S = \int d^4x\sqrt{-g}\left[\frac{1}{16\pi G}(R - 2\Lambda) + \mathcal{L}_M\right] \tag{2.5}$$

Here, g is the determinant of the metric tensor $g_{\mu\nu}$, R is the Ricci scalar, Λ is the cosmological constant, and $\mathcal{L}_M$ is the matter Lagrangian density. Varying this action with respect to the metric tensor yields the Einstein field equations. The energy-momentum tensor is derived from the matter action S_M as:

$$T_{\mu\nu} = -\frac{2}{\sqrt{-g}}\frac{\delta S_M}{\delta g^{\mu\nu}}, \quad \text{with} \quad S_M = \int d^4x\sqrt{-g}\mathcal{L}_M \tag{2.6}$$

The solutions to the Einstein field equations define the metric of the spacetime manifold, which in turn determines the geodesics—paths followed by free-falling particles. The simplest cosmological solution consistent with the Cosmological Principle is described by the Friedmann-Lemaître-Robertson-Walker (FLRW) metric, which led to the derivation of the Friedmann equations in 1922 by Alexander Friedmann, governing the expansion dynamics of the universe.

General Relativity, as a classical field theory, provides accurate predictions for various astrophysical and cosmological phenomena, including gravitational lensing, black holes, and the time dilation effects near massive objects. Its predictions have been confirmed extensively, establishing it as a foundational theory in modern physics.

2.3 Friedmann–Lemaître–Robertson–Walker(FLRW) Metric

The foundation of physical cosmology is rooted in the *cosmological principle*, which asserts that the Universe is homogeneous and isotropic when viewed on sufficiently large scales, typically greater than 100 megaparsecs (Mpc). Homogeneity implies that the Universe appears the same from every spatial location, while isotropy indicates that the Universe looks the same in all directions. Although isotropy does not necessarily imply homogeneity, the Copernican principle—the assumption that the Earth does not occupy a special position in the Universe—allows isotropy about every point to imply homogeneity.

Observational evidence supports both these assumptions. The Cosmic Microwave Background Radiation (CMBR) serves as strong evidence for isotropy, while the large-scale distribution of galaxies substantiates homogeneity. Under the framework of the cosmological principle, the curvature of spacetime is constant across spatial coordinates but may evolve over time. An exact solution to Einstein's gravitational field equations that adheres to these symmetries is described by the *Friedmann–Lemaître–Robertson–Walker (FLRW) metric*.

The FLRW metric defines a four-dimensional spacetime that can be foliated into three types of constant-curvature spatial hypersurfaces: flat, spherical, or hyperbolic. The general form of the FLRW metric is:

$$ds^2 = -c^2 dt^2 + a^2(t) \left[\frac{dr^2}{1 - \frac{kr^2}{R_0^2}} + r^2 d\theta^2 + r^2 \sin^2\theta \, d\phi^2 \right] \tag{2.7}$$

Alternatively, in natural units where $c = 1$, it simplifies to:

$$ds^2 = -dt^2 + a^2(t) \left[\frac{dr^2}{1 - kr^2} + r^2(d\theta^2 + \sin^2\theta \, d\phi^2) \right] \tag{2.8}$$

Here, $a(t)$ is the *scale factor*, which governs the expansion of the Universe as a function of cosmic time t. The coordinates (r, θ, ϕ) are the *comoving coordinates*, which remain fixed for observers moving with the Hubble flow. The physical (proper) radial distance is given by $r_{\text{physical}} = a(t)r$, and thus the physical velocity becomes:

$$v_{\text{physical}} = \frac{d}{dt}(a(t)r) = \dot{a}(t)r + a(t)\frac{dr}{dt} = Hr_{\text{physical}} + v_{\text{peculiar}} \qquad (2.9)$$

where the *Hubble parameter* is defined as:

$$H = \frac{\dot{a}}{a} \qquad (2.10)$$

The term Hr_{physical} corresponds to the *Hubble flow*, which arises due to the expansion of space itself, while v_{peculiar} denotes the *peculiar velocity*—the motion of a galaxy relative to the Hubble flow, as measured by a comoving observer.

The curvature parameter k determines the geometry of the spatial sections:

$$k = \begin{cases} +1 & \text{(spherical geometry)} \\ 0 & \text{(flat geometry)} \\ -1 & \text{(hyperbolic geometry)} \end{cases}$$

The quantity R_0 represents the curvature radius in the case of non-zero curvature. The FLRW metric reflects the high degree of symmetry in the Universe, though this symmetry is not always evident from the coordinate form of the metric itself. Nonetheless, the physical quantities derived from it exhibit full isotropy and homogeneity.[4]

Two characteristic scales are associated with the FLRW cosmology: the *Ricci scalar curvature radius*, $R = a|k|^{-1/2}$, and the *Hubble time*, $t_H = H^{-1}$, both of which evolve over time, revealing the dynamic nature of the Universe. The FLRW metric, therefore, forms the basis for modeling the large-scale structure and temporal evolution of the cosmos in modern cosmology.[5]

2.4 Friedmann Equations

The dynamics of the universe's expansion are governed by the Friedmann equations, derived from Einstein's field equations under the assumption of a homogeneous and isotropic universe

described by the Friedmann-Lemaître-Robertson-Walker (FLRW) metric. For a perfect fluid, the energy-momentum tensor is given by:

$$T_{\mu\nu} = (\rho + p)u_\mu u_\nu + pg_{\mu\nu},$$

where ρ is the energy density, p is the pressure, and u_μ is the four-velocity of the fluid.

The **first Friedmann equation**, describing energy conservation in an expanding universe, is:

$$H^2 + \frac{k}{a^2} = \frac{8\pi G}{3}\rho,$$

with $H = \frac{\dot{a}}{a}$ as the Hubble parameter, $a(t)$ the scale factor, k the curvature parameter, and G Newton's gravitational constant. This equation relates the expansion rate of the universe to its total energy density.

For a spatially flat universe ($k = 0$), the corresponding **critical density** is:

$$\rho_c = \frac{3H^2}{8\pi G}.$$

If the actual density ρ equals ρ_c, the universe is flat. A density $\rho > \rho_c$ implies a closed universe with spherical geometry, while $\rho < \rho_c$ indicates an open universe with hyperbolic geometry.

The **second Friedmann equation**, which includes the effect of pressure, is:

$$2\dot{H} + 3H^2 + \frac{k}{a^2} = -8\pi G p.$$

From the first and second Friedmann equations, the **acceleration equation** is derived as:

$$\frac{\ddot{a}}{a} = -\frac{4\pi G}{3}(\rho + 3p).$$

This expression shows that the acceleration of the universe's expansion is influenced by both the energy density and pressure of its contents. The pressure and density are related via

the **equation of state parameter** ω, defined by:

$$\omega = \frac{p}{\rho}.$$

Within the ΛCDM framework, the universe is composed of matter (including baryonic and dark matter), radiation, and dark energy. Observational evidence suggests that only about 5% of the universe's energy density is in the form of ordinary matter and radiation, while the remaining 95% consists of non-luminous components: **dark matter**, which shapes large-scale structures, and **dark energy**, which is responsible for the universe's current accelerated expansion.

2.5   Dark Energy

The ΛCDM model introduces dark energy through the cosmological constant Λ, which has an extremely small value on the order of $\sim 10^{-52}$ m^{-2}. Dark energy is a mysterious form of energy that dominates the present energy content of the universe and is responsible for its observed accelerated expansion. This acceleration, first confirmed by observations of Type Ia supernovae, requires the presence of a component with negative pressure.

In the standard cosmological framework, a cosmological constant is a natural candidate for dark energy. It corresponds to an equation of state parameter $\omega_\Lambda = -1$, which implies that its pressure and energy density are related by $p_\Lambda = -\rho_\Lambda$. The energy density associated with the cosmological constant is given by:

$$\rho_\Lambda = \frac{\Lambda}{8\pi G}$$

where G is the gravitational constant. In natural units, since the pressure is negative, the expansion of the universe performs work on Λ, yet its energy density remains constant as the universe expands.

Dark energy only began to dominate the cosmic dynamics in the recent epoch. A general

requirement for a component to cause cosmic acceleration is that its equation of state parameter satisfies $-1 \leq \omega \leq -\frac{1}{3}$. The cosmological constant, with a constant $\omega = -1$, remains the simplest and most successful model for dark energy, despite the lack of understanding of its physical origin.

In a flat ΛCDM universe, where the spatial curvature $k = 0$ and the radiation density parameter Ω_r is negligible at late times, the Friedmann equation simplifies to:

$$H = H_0 \sqrt{\Omega_m a^{-3} + \Omega_\Lambda}$$

Given that $\Omega_m + \Omega_\Lambda = 1$ for a flat universe, this can also be written as:

$$H = H_0 \sqrt{\Omega_m a^{-3} + (1 - \Omega_m)}$$

Here, Ω_m and Ω_Λ are the matter and dark energy density parameters, respectively, and H_0 is the Hubble constant.

2.6 Dark Matter

Dark matter is a form of matter that does not interact electromagnetically, making it invisible to telescopes. It was first postulated by Fritz Zwicky in 1937, who noticed that the visible mass in galaxy clusters was insufficient to account for their observed gravitational effects. He concluded that most of the mass was in a non-luminous form, which came to be known as dark matter.[7]

Modern astrophysical evidence supports the dominance of dark matter in the universe. It plays a critical role in the dynamics of galaxies and galaxy clusters. Its presence is inferred through several phenomena, including galaxy rotation curves, gravitational lensing

Chapter 3

Hubble tention and fixing of absolute magnitude

3.1   Hubble Tension

One of the most actively debated issues in modern cosmology is the discrepancy in the measurements of the Hubble–Lemaître constant H_0, commonly referred to as the "Hubble tension." This term describes the significant and persistent difference between the value of H_0 obtained from observations of the local universe and the value inferred from early universe measurements assuming the standard ΛCDM cosmological model.in figure 3.1 Histogram and scatter diagram of 216 measurements of the Hubble–Lemaître constant H0 between 2012 and 2022. The size of the blue scatter points is inversely proportional to the error. Obviously, there is potential for increasingly precise estimation of H0. The red points are weighted averages with weighted standard deviations for each year. The results derived from the local Cepheid-supernova distance ladder and CMB data are also included for comparison.

The tension gained widespread attention following the 2019 study by Riess et al., which reported a local value of $H_0 = 74.0 \pm 1.4 \, \mathrm{km \, s^{-1} Mpc^{-1}}$ using Cepheid-calibrated Type Ia supernovae. This was in stark contrast with the value derived from observations of the Cosmic Microwave Background (CMB) by the Planck satellite, which yielded $H_0 = 67.4 \pm 0.5 \, \mathrm{km \, s^{-1} Mpc^{-1}}$ (Planck Collaboration, 2020), assuming a flat ΛCDM model. The difference
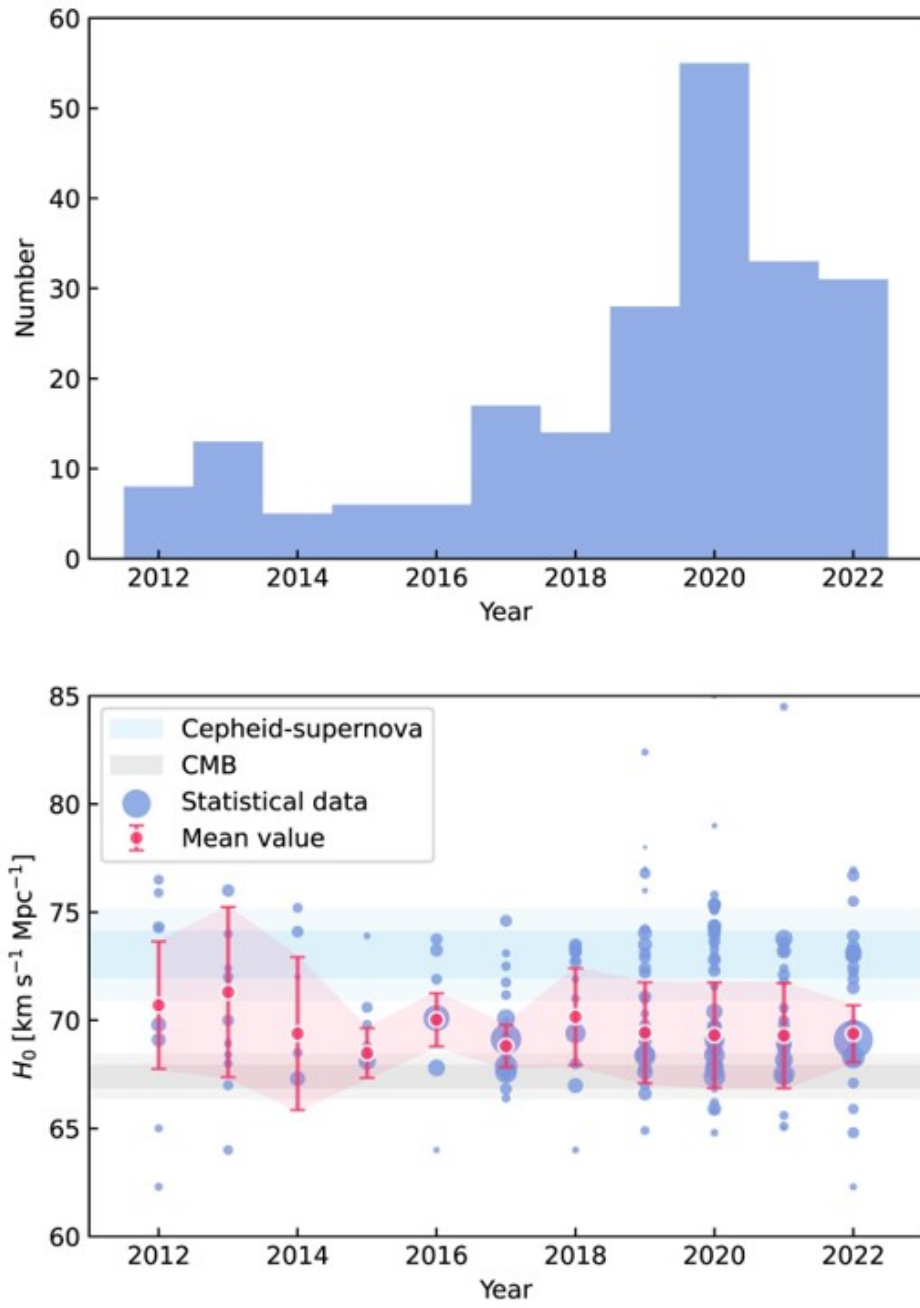
Figure 3.1: Hubble Tension

between these two measurements corresponds to a statistical tension at the 4.4σ level. Subsequent analyses increased this tension to nearly 6σ, depending on the dataset combinations (Di Valentino et al. 2021).

The most recent measurement from Riess et al. (2022) has refined the local estimate to $H_0 = 73.04 \pm 1.04 \, \mathrm{km \, s^{-1} Mpc^{-1}}$, now differing from the CMB-inferred value by a full 5σ. This increasing level of statistical inconsistency has led to extensive theoretical and observational scrutiny, including the exploration of possible new physics beyond the ΛCDM paradigm, as well as more precise investigation into observational methods.

However, such discrepancies in H_0 measurements are not unprecedented. Historical data from earlier decades show significant variability in the estimated values of the Hubble constant. Prior to the 1970s, differing approaches to calibrating standard candles often led to wide discrepancies. Over time, values of H_0 decreased as improved methodologies and better corrections for systematic errors were implemented. Even after the 1970s, persistent variations have continued to appear in published measurements.

Studies such as Chen, Gott, and Ratra (2003) showed that the distribution of measured H_0 values up to the early 2000s exhibited strong non-Gaussian behavior, with much larger tails than expected from normal error statistics. This indicated that systematic uncertainties were likely dominating the errors. Gott et al. (2001) estimated that these systematics could contribute uncertainties on the order of $\sim 5 \, \mathrm{km \, s^{-1} Mpc^{-1}}$ at the 95% confidence level.

Standard statistical analyses often assume Gaussian error distributions, as motivated by the central limit theorem. However, more recent investigations (Faerber & López-Corredoira 2020; López-Corredoira 2022) analyzing the distribution of H_0 values from 1976 to 2019 found that the empirical error distributions exhibit far greater spread than would be expected under Gaussian assumptions. This suggests that quoted uncertainties are often underestimated, or that systematic effects have not been adequately accounted for.

In fact, recalibrations of these results indicate that tensions reported at 4.4σ and 6.0σ under standard Gaussian assumptions could correspond to only 2.1σ and 2.5σ discrepancies, respectively, in terms of actual frequency distributions. This would imply that such differences are

more common than previously believed and might not signify a true breakdown of the underlying cosmological model, but rather reflect persistent issues with error estimation.

To further investigate this issue, our current work focuses on an updated statistical analysis of Hubble constant measurements restricted to the period 2012–2022. Although systematic and statistical errors have improved significantly over past decades, it remains valuable to test whether the overall distribution of published H_0 values conforms to expectations based on Gaussian statistics. While the specific tension between Type Ia supernova data and CMB-inferred values remains a prominent outlier, this study aims to evaluate the broader statistical behavior of all available measurements during this recent decade. A number of schemes have been proposed to explain or resolve the H0 tension. In general, these fall into two categories (i) the difference is due to unresolved or unknown systematics in the analyses of the higher-redshift CMB data and/or some of the lower-redshift local distance-ladder data; or (ii) the difference indicates that the standard flat ΛCDM model is an inadequate cosmological model. The second category includes a variety of proposed cosmological models, some with modified, relative to flat ΛCDM, low-redshift, or late-time evolution, e.g., some modified gravity theories[17]

3.2   The SH0ES Program

The present expansion rate of the universe, quantified by the Hubble constant (H_0), defines the fundamental scale of the universe in terms of both its size and age. It establishes the relationship between redshift—a direct consequence of cosmic expansion—and physical distance and time.

The value of H_0 can be determined in two principal ways. Locally, it is measured by combining observations of distances and redshifts of nearby galaxies, utilizing standard candles such as Cepheid variables and Type Ia supernovae. Alternatively, H_0 can be inferred from the early universe by calibrating a cosmological model using observations of the cosmic microwave background (CMB), corresponding to the epoch of recombination at redshift $z \approx 1100$.

A comparison between the locally measured and model-predicted values of H_0 offers a powerful, end-to-end test of cosmological models. This comparison spans the universe's entire

evolutionary history—from the dense, radiation- and dark matter-dominated conditions of the early universe to the current era, which is increasingly governed by dark energy. Discrepancies between these two determinations of H_0 have profound implications, potentially signaling new physics beyond the standard ΛCDM cosmological model.[12]

3.3 Work Undertaken in SH0ES program and Mitigation of Practical Errors

This project, conducted under the SH0ES program, represents the most comprehensive and precise effort to date to locally determine the Hubble constant (H_0) using a three-step distance ladder approach. The team expanded the number of calibrator Type Ia supernovae (SNe Ia) from 19 in the previous Riess et al. (2016) work to a total of 42, observed across 37 distinct host galaxies. These objects span redshifts of $z < 0.011$, capturing all known, viable SNe Ia within this range, with two additional supernovae slightly beyond the threshold added to test the robustness of the distance calibration range. The expanded SN sample enhances the statistical power of the analysis, which was previously limited by the small size of the calibrator set.

The three-step ladder used to measure H_0 consists of: (1) geometric distances (e.g., to NGC 4258 via water masers) used to calibrate Cepheid variable stars, (2) Cepheid distances used to calibrate SNe Ia in nearby host galaxies, and (3) these calibrated SNe Ia used to measure the expansion rate of the universe through observations in the Hubble flow. All steps are fit simultaneously using a minimization framework χ^2, which incorporates measurement uncertainties and covariances, including those from SN Ia data (SNcov), metallicity dependencies (Zcov) and background effects ($C_{i,j,k,\text{bkgd}}$). The final output includes the best-fit values of several key parameters: the fiducial luminosity of Cepheids and SNe Ia, the Cepheid period and metallicity dependence, and H_0 itself.

The project made extensive use of high-quality HST photometry to identify and measure classical Cepheid variables. These stars were discovered in both new and existing fields using a campaign of visual-band observations spaced over 60–100 days, enabling precise period

measurements through their distinctive light curves. Over 60,000 individual measurements in filters like F555W and F350LP were compiled to construct composite light curves, exhibiting the classic sawtooth shapes expected of fundamental-mode pulsators. The detection of subtle features such as the Hertzsprung progression (including the "bumpphenomenon " caused by resonance between pulsation modes) provided strong validation of the physical consistency of the Cepheid sample with known Galactic Cepheids.

Photometric systematics were rigorously controlled. The project used near-infrared (NIR) imaging to reduce the effects of dust extinction, and refined all NIR photometry using reprocessed HST data with updated calibrations, including new flat fields and distortion corrections. The point spread function (PSF) for photometry was modeled empirically from the solar analog P330E, and each Cepheid's photometric environment was tested with 100 artificial stars to estimate and correct for crowding biases and background uncertainties. Additionally, light curves and positions from optical observations were used to precisely locate the same stars in the NIR data, minimizing position-based errors.

To ensure the universality and reliability of Cepheid standardization across host galaxies, the team tested for consistency in light-curve morphology and metallicity response. They performed multiple independent checks on Cepheid PSF photometry and background estimates. These efforts ensured that both the Cepheid data and SN Ia observations contributed to a robust calibration framework for determining H_0 with reduced systematic and statistical errors.[12]

3.4   Fixing the Absolute Magnitude of Type Ia Supernovae

The cornerstone of this study is the accurate determination of the absolute magnitude of Type Ia supernovae (M), which enables their use as standard candles for cosmological distance measurement. In the distance ladder framework, this is achieved by comparing the observed brightness of nearby SNe Ia with the distances to their host galaxies, which are independently established through Cepheid variable stars.

The fundamental relationship that connects redshift (z) to distance (D) in an expanding uni-

verse is given by $cz = H_0 D$, where c is the speed of light. To determine the distances required for this relation, the project applies a hierarchical calibration: first, geometric distances to anchor galaxies like NGC 4258 are used to fix the Cepheid period-luminosity relation; second, Cepheids in SN Ia host galaxies provide distances to those galaxies; and third, the apparent magnitudes of the hosted SNe Ia are used to calibrate their absolute magnitudes. This enables the use of high-redshift SNe Ia as reliable probes of cosmic expansion.

The process of fixing the SN Ia absolute magnitude involves fitting a system of linear equations encompassing all observed quantities and their uncertainties. These include Cepheid periods, metallicities, and fluxes (expressed in Wesenheit magnitudes to account for reddening), as well as SN Ia peak magnitudes corrected for light-curve shape and color. The Cepheid Wesenheit magnitude relation is of the form:

$$m_{W,ij} = M_{W,1} + b_W(\log P_{ij} - 1) + Z_W[\text{O/H}]_{ij} + \mu_i \tag{3.1}$$

Here, $M_{W,1}$ is the fiducial absolute magnitude for a Cepheid with a 10-day period and solar metallicity, while b_W and Z_W characterize the dependence of Cepheid luminosity on period and metallicity, respectively. μ_i is the distance modulus of the host galaxy. The derived SN Ia magnitudes are then tied to this calibrated distance scale. All of these parameters are optimized simultaneously by minimizing a χ^2 statistic, accounting for all known sources of uncertainty and covariance.

The simultaneous fit outputs the most likely value of the SN Ia fiducial luminosity (M_{SN}), which in turn provides the normalization needed to translate SN Ia apparent magnitudes at cosmological distances into physical distances. This calibration is crucial because even a small error in M_{SN} can lead to significant discrepancies in H_0. The robustness of the method is further reinforced by an independent Markov Chain Monte Carlo (MCMC) sampling of the likelihood space, confirming that the best-fit values from the analytical solution are consistent across methodologies.

The final value of the SN Ia absolute magnitude derived in this study is based on the largest

and most systematically treated set of calibrator SNe Ia and Cepheids to date. The combination of carefully selected data, rigorous photometric analysis, correction for metallicity effects, and simultaneous statistical optimization ensures that this value is both precise and reliable. It is this calibration that underpins the updated and more accurate measurement of the Hubble constant, providing a solid local benchmark for comparing to early-universe predictions.[12]

3.5 Bayes' Theorem

Bayes' Theorem emerges naturally from the basic axioms of probability theory and provides a systematic way to update our beliefs in light of new information. While its mathematical form is universally accepted, debates continue regarding its philosophical implications — particularly its application in inference and decision-making under uncertainty.

The strength of Bayes' Theorem lies in its grounding in logic. It is not just a rule of probability, but a consequence of deeper consistency requirements for rational reasoning, known as Cox's axioms. These axioms show that Bayesian probability is the unique and coherent extension of Boolean logic when dealing with uncertain propositions. In essence, Bayesian inference is the formalization of logical deduction in situations where complete information is not available.

To build the mathematical framework, let us consider a proposition A, which may represent a random variable (e.g., the outcome of rolling two dice) or a single-event statement (e.g., a future event like a royal succession). The sum rule of probability asserts that:

$$p(A \mid I) + p(\bar{A} \mid I) = 1,$$

where I represents the background information assumed to be true.

The product rule describes joint probabilities:

$$p(A, B \mid I) = p(A \mid B, I) \cdot p(B \mid I).$$

This tells us that the probability of both A and B occurring is the probability of A given B, multiplied by the probability of B, each conditional on the same background information.

If we want the probability of B alone (without concern for A), we apply the marginalization principle:

$$p(B \mid I) = \sum_A p(A, B \mid I).$$

Combining the product rule and the symmetry of joint probabilities, we arrive at the core result:

$$p(B \mid A, I) = \frac{p(A \mid B, I) \cdot p(B \mid I)}{p(A \mid I)},$$

which is Bayes' Theorem.

To interpret this more practically, consider replacing A with observed data d, and B with a hypothesis H. The theorem becomes:

$$p(H \mid d, I) = \frac{p(d \mid H, I) \cdot p(H \mid I)}{p(d \mid I)}.$$

In this form, $p(H \mid d, I)$ is the posterior probability — our updated belief in the hypothesis after observing the data. $p(d \mid H, I)$ is the likelihood — the probability of observing the data assuming the hypothesis is true. $p(H \mid I)$ is the prior — our belief in the hypothesis before seeing the data. $p(d \mid I)$, also called the marginal likelihood or Bayesian evidence, ensures normalization and is crucial for comparing different models.

Although the likelihood reflects how the data supports various hypotheses, it is not itself a probability distribution over hypotheses. The posterior, however, directly represents our revised belief in each hypothesis after accounting for the observed evidence.

One of the key insights of Bayes' Theorem is its directionality: it provides a logical path from prior knowledge to updated beliefs, emphasizing how we learn from experience. Notably, the prior does not need to be specified before data is gathered; it must only represent belief

independent of the current dataset. This flexibility supports scientific reasoning rather than undermining it.

Critics often challenge Bayesian inference for its subjectivity, citing the need to choose a prior. However, this requirement is not a weakness but a reflection of scientific transparency. Rather than obscuring assumptions, Bayesian methods make them explicit and logically consistent. In fact, Bayesian probability is arguably the most principled approach to updating beliefs based on new information.

The SH0ES program has modified the Pantheon data by adding the absolute magnitude value of Type Ia supernovae. By using the relation

$$\mu_{\text{th}}(z) = m(z) - M \tag{3.2}$$

and the value of the absolute magnitude, which is -19.253 ± 0.03, they constructed a data of distance modulus. Here this project, we will constrain the hubble constant buy taking the apparent magnitude data and the distance modulus data.[16]

3.6 Markov Chain Monte Carlo Methods

Markov Chain Monte Carlo (MCMC) techniques are powerful computational tools widely used for the analysis of complex data, particularly in cosmology for constraining model parameters. These methods have become essential in modern numerical analysis, especially for comparing theoretical models against observational data.

MCMC methods combine two fundamental statistical techniques: Markov chains and Monte Carlo simulations. A Markov chain is defined as a sequence of random variables

$$\{X^{(0)}, X^{(1)}, \ldots, X^{(M-1)}\} \tag{3.3}$$

where the probability of transitioning to the $(t+1)$-th state depends solely on the current state $X^{(t)}$. On the other hand, Monte Carlo methods are used for random sampling from a

specified probability distribution.

In the context of MCMC, Monte Carlo simulations are employed to draw samples from a Markov chain after it has reached convergence. It can be mathematically shown that Markov chains converge to a stationary distribution, at which point the successive samples are effectively drawn from the target distribution—in this case, the posterior distribution of the model parameters.

Several algorithms are available for generating Markov chains suitable for MCMC analysis. The choice of algorithm depends on the specific problem being addressed. Commonly used algorithms include the Metropolis-Hastings algorithm, Gibbs sampling, and Hamiltonian Monte Carlo.

The Markov chain explores the parameter space in search of the maximum likelihood. The basic procedure involves selecting a random initial point in the parameter space and proposing a random step or jump. If the new point yields a higher likelihood, the jump is accepted; otherwise, it may be rejected based on a probabilistic criterion. This process is iterated, allowing the chain to explore the region of highest posterior probability.

Care must be taken when choosing the size of the steps. If the steps are too large, the algorithm may struggle to find regions of higher likelihood, possibly getting trapped in local maxima. Conversely, if the steps are too small, the chain may explore the space too slowly, requiring significantly more iterations. To mitigate these issues, it is often beneficial to run multiple chains from different starting points to ensure convergence to the global maximum.

Compared to earlier grid-based methods, MCMC is significantly more efficient, especially in high-dimensional parameter spaces. Once a Markov chain has been generated, the expectation value of any function of the parameters can be estimated. For example, the posterior mean of a parameter θ is approximated by:

$$\langle \theta \rangle \approx \int p(\theta|d)\theta \, d\theta \approx \frac{1}{M} \sum_{t=0}^{M-1} \theta^{(t)}, \tag{3.4}$$

where $p(\theta|d)$ is the posterior distribution given the observed data d, and M is the number

of samples in the chain.

Similarly, the expectation value of a function $f(\theta)$ is given by:

$$\langle f(\theta) \rangle \approx \frac{1}{M} \sum_{t=0}^{M-1} f(\theta^{(t)}). \tag{3.5}$$

These statistical estimates form the foundation for parameter inference and uncertainty quantification in cosmological and other scientific analyses using MCMC.[16]

3.7   Parameter estimation

The SH0ES program has modified the Pantheon data by adding the absolute magnitude value of Type Ia supernovae. By using the relation

$$\mu_{\text{th}}(z) = m(z) - M \tag{3.6}$$

Here along with the hubble constant H_0 and energy density Ω_{m} the absolute magnitude would be a free parameter. Whereas using the value of the absolute magnitude, which is -19.253 ± 0.03, they constructed a data of distance modulus. Here this project, we will constrain the hubble constant buy taking the apparent magnitude data and the distance modulus data.

To estimate the model parameters We perform Markov Chain Monte Carlo (MCMC) analysis by minimizing the χ^2 in the light of observational data. Here, we use the combined dataset, SNIa + BAO + OHD for the parameter inference. The largest spectroscopically conformed, Type Ia supernovae data set is the Pantheon+ sample includes 1701 light curves of 1550 distinct Type Ia supernovae (SNe Ia) in the redshift range $0.001 < z < 2.26$. To compute χ^2 we compare the apparent magnitude observed with the theoretical magnitude calculated from the model. The luminosity distance dL of the k-th supernova with redshift zi in a flat universe is defined as

$$dL(z) = c(1 + z) \int_0^z \frac{dz}{H(z)} \tag{3.7}$$

H(z) is the hubble parameter and c is the speed of the light. The theoretical apparent magnitude

is estimated using the equation.

$$m(z) = 5 \log_{10} \left(\frac{dL(z)}{\text{Mpc}} \right) + 25 + M \tag{3.8}$$

where M is the absolute magnitude of the Type Ia supernova, a nuisance parameter. We compare the apparent magnitude of Type Ia supernovae with the corresponding theoretical one to obtain the χ^2_{SNIa}.

$$\chi^2 = \Delta m^T \cdot C^{-1} \cdot \Delta m \tag{3.9}$$

where

$$\Delta m = m(z) - m_{data} \tag{3.10}$$

BAO measurements are very important observational probes in cosmology as its peak location is commonly realized as a fixed co-moving ruler. The cosmological parameters used to calibrate the characteristic BAO scale r_d are typically derived from CMB observations. The r_d scale can also be derived from Big Bang Nucleosynthesis (BBN) measurements (which provide constraints on ω_b) in combination with measurements of the expansion history (which provide constraints on Ω_m), assuming that the early Universe is a mixture of radiation, baryonic matter, and cold dark matter with three neutrino species. With a calibrated r_d, the BAO scale can be used to make absolute distance measurements as a function of redshift. Alternatively, r_d can be treated as a nuisance parameter, allowing multiple BAO measurements over a range of redshifts to be used for relative measures of the cosmic expansion history.

In a spectroscopic survey, the BAO feature appears in both the line-of-sight direction and the transverse direction. Along the line-of-sight direction, a measurement of the redshift interval Δz, over which the BAO feature extends, provides a means to directly measure the Hubble parameter:

$$H(z) = \frac{c \Delta z}{r_d}$$

Equivalently, this measures the Hubble distance at redshift z. BAO measurements include the transverse comoving distance defined as

$$D_M(z) = D_c(z) = c \int_0^z \frac{dz'}{H(z')} \tag{3.11}$$

Angular diameter distance, Other useful physical quantities which can be defined as

$$DA(z) = \frac{DM(z)}{1 + z} \tag{3.12}$$

volume-averaged angular diameter distance, which can be written as

$$DV(z) = \left(\frac{czD_M^2(z)}{H(z)} \right)^{1/3} \tag{3.13}$$

Hence we obtain the χ^2_{BAO}

We have used 8 data points in the redshift range $0.38 \leq z \leq 1.52$, presented in Ref. 90. We use the Observational Hubble Data (OHD), which includes 43 data points in the redshift range $0.0708 \leq z \leq 2.36$ to obtain χ^2_{OHD}.

To estimate the free parameters in the 2nd method were we use the distance modulus data, absolute magnitude is not a free parameter . Hence the Δm will be replaced with

$$\Delta m = \mu(z) - \mu_{data} \tag{3.14}$$

where $\mu(z)$ can be written as

$$\mu(z) = 5 \log_{10} \left(\frac{dL(z)}{\text{Mpc}} \right) + 25 \tag{3.15}$$

Then, the χ^2 corresponding to each data set, other than pantheon+, can be calculated using the equation

$$\chi^2(H_0, \Omega_m) = \sum_k \left[\frac{E(H_0, \Omega_m, z_k) - O_k}{\sigma_k} \right]^2$$

where O_k is the physical quantity obtained from the data at redshift z_k, E is the correspond-

ing physical quantity obtained from the model, and σ_k is the corresponding standard deviation in the measurement. The parameters that best fit the data combination SNe Ia + BAO + OHD are obtained by minimizing the χ^2 of the form:

$$\chi^2_{\text{total}} = \chi^2_{\text{SNeIa}} + \chi^2_{\text{BAO}} + \chi^2_{\text{OHD}} \tag{3.16}$$

[13] In order to make sure that the results obtained are not model dependent, we have considered 2 other CDM models, wCDM and CPL Parametrization

w**CDM**

The wCDM model is a simple extension of the standard cosmological model, ΛCDM. Like ΛCDM, it includes the Big Bang framework, cold dark matter (CDM), and dark energy. However, instead of assuming that dark energy is a cosmological constant Λ, the wCDM model allows the dark energy component to have a constant but free equation of state parameter, denoted as w, defined by the ratio of its pressure p to energy density ρ:

$$w = \frac{p}{\rho}$$

In this model, w is not fixed at -1, as in the case of a cosmological constant, but is treated as a parameter to be determined from observations. This allows for a more flexible approach to describing the behavior of dark energy over cosmic time.

The wCDM model retains the overall simplicity and assumptions of general relativity and cold dark matter, but introduces an extra degree of freedom to explore deviations from the standard ΛCDM scenario. It is often used as a benchmark model when testing whether the data favor a more dynamic form of dark energy, while still keeping the framework manageable and consistent with current observations.[9]

$$\sqrt{(om(1+z)^3 + (1-om)(1+z)^{(3(1+w))})} \tag{3.17}$$

CPL Parametrization

The Chevallier-Polarski-Linder (CPL) parameterization is a widely used model for describing the equation of state $w(z)$ of dark energy, which is the ratio of dark energy's pressure to its energy density. The model is defined by the equation:

$$w_{\text{CPL}}(z) = w_0 + w_a \frac{z}{1+z},$$

where w_0 and w_a are free parameters. The parameter w_0 represents the present value of the equation of state, while w_a describes its evolution over time. This simple yet effective form allows us to describe dark energy's behavior across different epochs of the universe.

The CPL model is particularly useful when comparing various observational probes of dark energy. It provides a way to fit a wide variety of scalar field models to the available data. One of the attractive features of the CPL parameterization is that the two parameters, w_0 and w_a, have clear physical interpretations. Moreover, the model exhibits interesting properties, such as a natural bounded behavior at high redshift, where the equation of state approaches a constant value.

Although the CPL parameterization is highly versatile, it is not able to capture all possible dark energy dynamics, particularly when exploring the full range of behaviors in the (w, w')-phase space. Despite this limitation, the CPL model remains a popular and practical choice for cosmological analyses because of its simplicity and its ability to describe the broad range of observed phenomena in the universe.[14]

$$\sqrt{((om)(1+z)^3) + (1-om)(1+z)^{3(1+w_0+w_a)} \exp(-3w_a z/(1+z))} \qquad (3.18)$$

Chapter 4

Result and Discussion

4.1   Results

Here we have used 6 types of data combinations and the 6 results obtained correspondingly

Data Combinations

Using Apparent Magnitude Data

Data 1 - Pantheon+ and OHD

Data 4 - Pantheon+ and OHD and BAO

Using Distance Modulus Data

Data 2 - Pantheon+

Data 3 - Pantheon+ and OHD

Data 5 - Pantheon+ and BAO

Data 6 - Pantheon+ and OHD and BAO

-	H_0	Ω_{m}	M_0
pantheon m OHD	$67.170^{+0.811}_{-0.809}$	$0.316^{+0.014}_{-0.013}$	$-19.445^{+0.023}_{-0.023}$
pantheon μ	$72.887^{+0.229}_{-0.229}$	$0.362^{+0.019}_{-0.018}$	-
pantheon μ OHD	$74.124^{+0.158}_{-0.160}$	$0.234^{+0.007}_{-0.007}$	-

Table 4.1: LCDM without BAO

-	H_0	Ω_{m}	r_d	M_0
pantheon m OHD	$67.451^{+0.689}_{-0.688}$	$0.311^{+0.011}_{-0.010}$	$149.224^{+1.273}_{1.269}$	$-19.437^{+0.020}_{-0.020}$
pantheon μ OHD	$73.921^{+0.151}_{-0.151}$	$0.247^{+0.006}_{-0.006}$	$143.115^{+1.041}_{-1.024}$	-
pantheon μ	$73.207^{+0.184}_{-0.186}$	$0.331^{+0.013}_{-0.013}$	$135^{+1.259}_{-1.248}$	-

Table 4.2: LCDM with BAO

-	H_0	Ω_{m}	M_0	w
w pantheon m OHD	$65.863^{+0.814}_{-0.814}$	$0.272^{+0.017}_{-0.017}$	$-19.465^{+0.022}_{-0.022}$	$-0.792^{+0.044}_{-0.044}$
w pantheon μ	$72.58^{+0.275}_{-0.267}$	$0.219^{+0.081}_{-0.096}$	-	$-0.715^{+0.116}_{-0.135}$
w pantheon μ OHD	$73.814^{+0.212}_{-0.212}$	$0.218^{+0.011}_{-0.011}$	-	$-0.854^{+0.049}_{-0.051}$

Table 4.3: WCDM without BAO

-	H_0	Ω_{m}	r_d	M_0	w
w BAO pantheon m OHD	$65.755^{+0.762}_{-0.752}$	$0.272^{+0.017}_{-0.017}$	$149.956^{+1.307}_{-1.206}$	$-19.476^{+0.021}_{-0.021}$	$-0.821^{+0.040}_{-0.040}$
w BAO pantheon μ OHD	$73.910^{+0.212}_{-0.212}$	$0.287^{+0.008}_{-0.008}$	$143.099^{+1.050}_{-1.020}$	-	$-0.998^{+0.031}_{-0.032}$
w BAO pantheon μ	$72.729^{+0.249}_{-0.248}$	$0.300^{+0.017}_{-0.017}$	$135.400^{+1.050}_{-1.020}$	−	$-0.854^{+0.049}_{-0.051}$

Table 4.4: WCDM with BAO

-	H_0	Ω_{m}	M_0	w_a	w_0
pantheon m OHD	$65.891^{+0.831}_{-0.832}$	$0.270^{+0.032}_{-0.088}$	$-19.464^{+0.024}_{-0.024}$	$0.010^{+0.571}_{-0.669}$	$-0.760^{+0.068}_{-0.057}$
pantheon μ	$72.475^{+0.303}_{-0.291}$	$0.317^{+0.064}_{-0.117}$	-	$-0.901^{+0.959}_{-0.767}$	$-0.746^{+0.111}_{-0.127}$
pantheon μ OHD	$72.274^{+0.290}_{-0.293}$	$0.235^{+0.007}_{-0.007}$	-	$-0.481^{+0.491}_{-0.518}$	$-0.651^{+0.077}_{-0.075}$

Table 4.5: CPL Parametrization without BAO

-	H_0	Ω_{m}	r_d	M_0	w_a	w_0
pantheon m OHD	$65.722^{+0.768}_{-0.760}$	$0.305^{+0.017}_{-0.026}$	$150.042^{+1.308}_{-1.300}$	$-19.466^{+0.022}_{-0.022}$	$-0.476^{+0.565}_{-0.530}$	$-0.771^{+0.067}_{-0.060}$
pantheon μ OHD	$72.618^{+0.259}_{-0.259}$	$0.231^{+0.007}_{-0.007}$	$135.023^{+1.284}_{-1.254}$	-	$0.490^{+0.160}_{-0.177}$	$-0.790^{+0.043}_{-0.043}$
pantheon μ	$72.339^{+0.313}_{-0.309}$	$0.337^{+0.018}_{-0.020}$	$136.188^{+1.318}_{-1.317}$	-	$-1.337^{+0.644}_{-0.681}$	$-0.726^{+0.088}_{-0.032}$

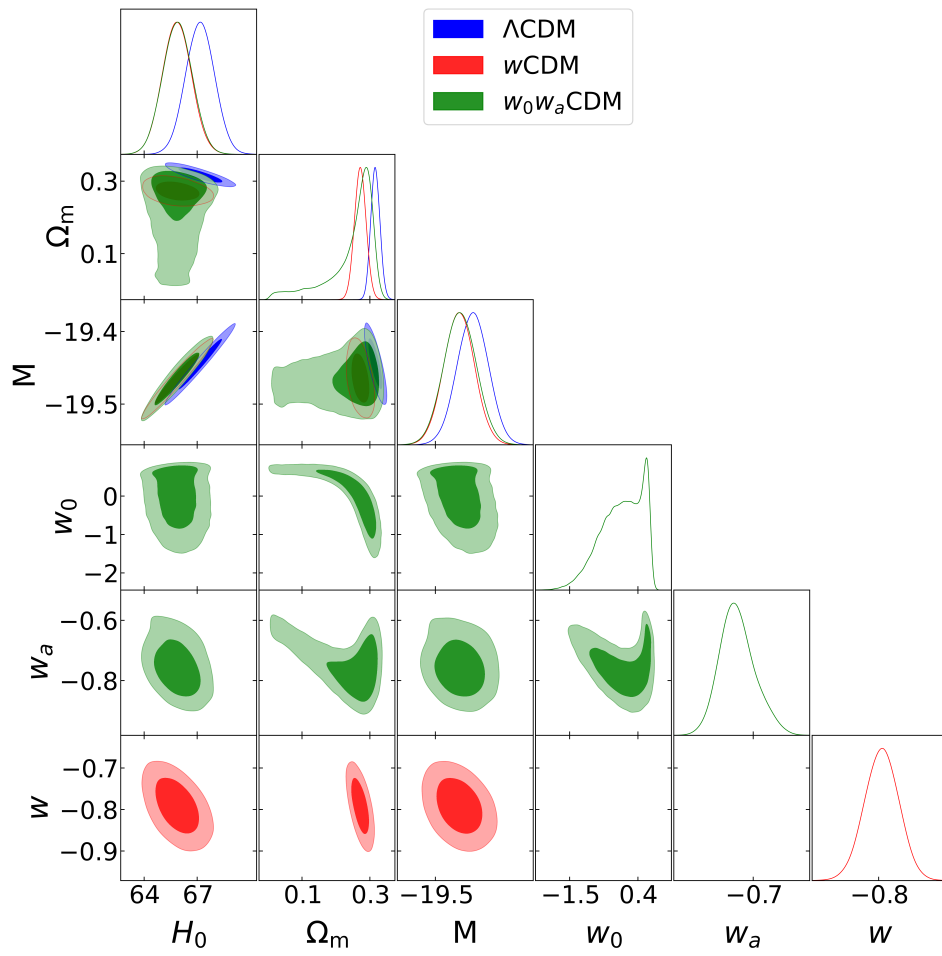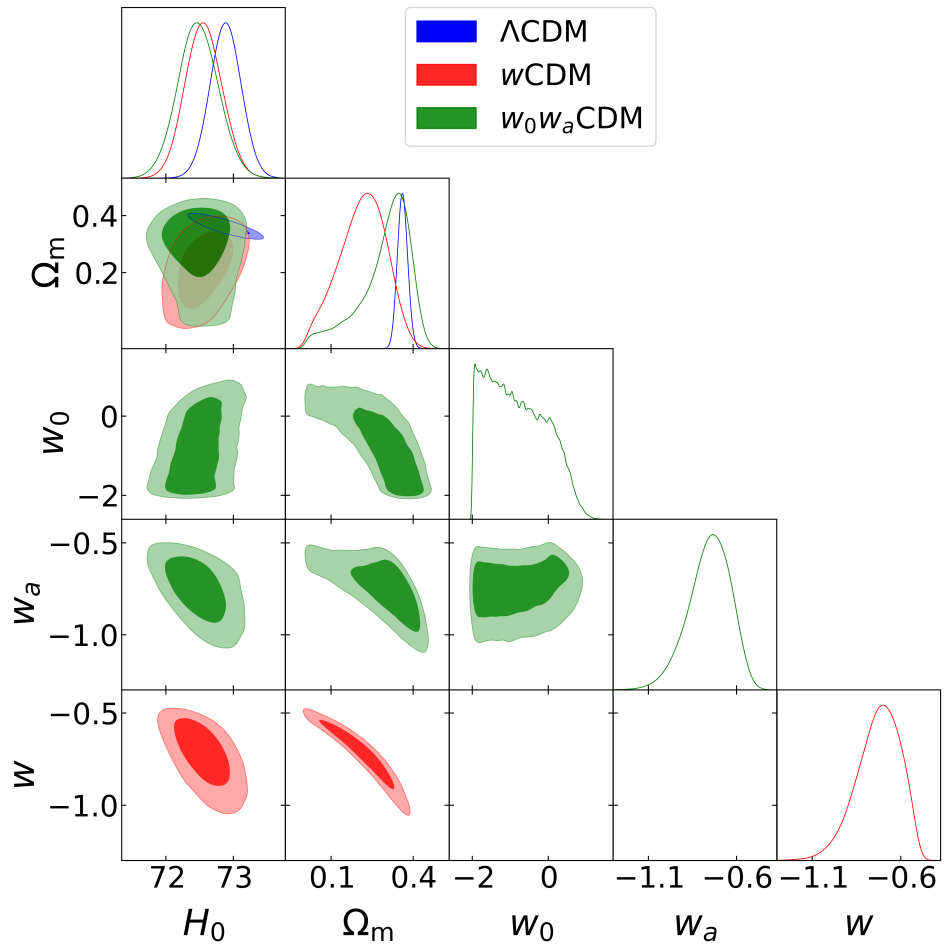Table 4.6: CPL Parametrization with BAO
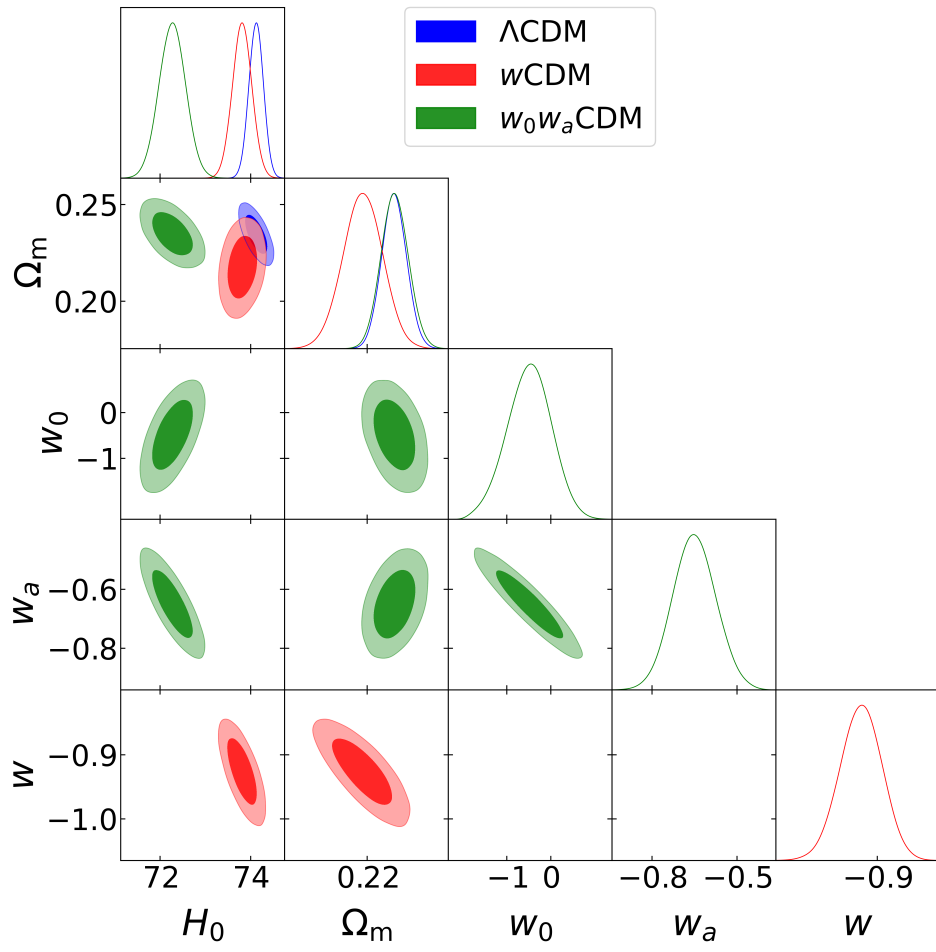
Figure 4.1: Data 1
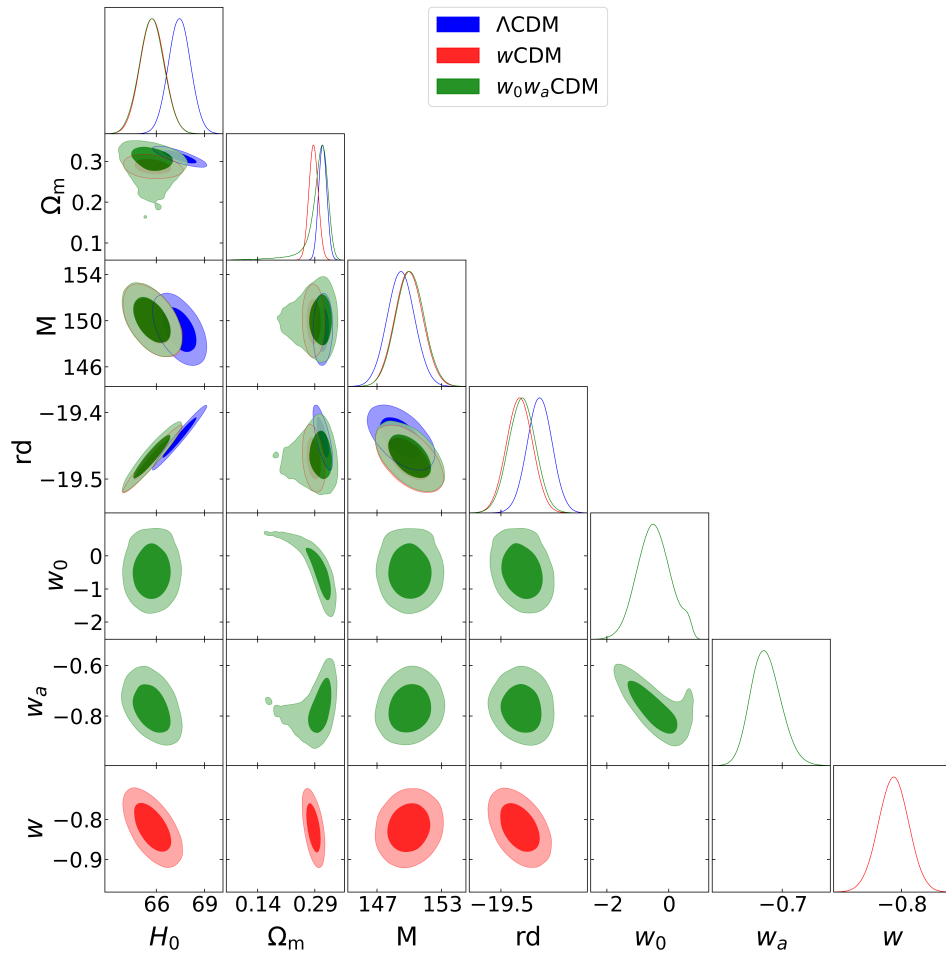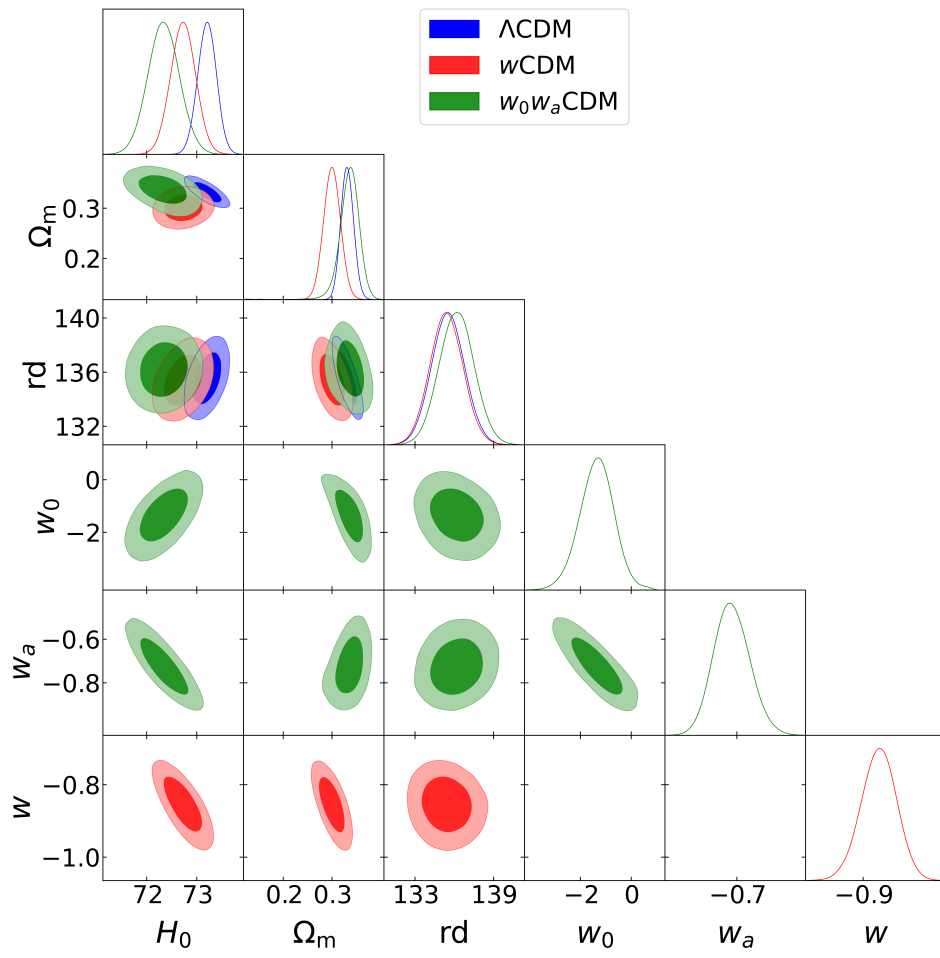
Figure 4.2: Data 2
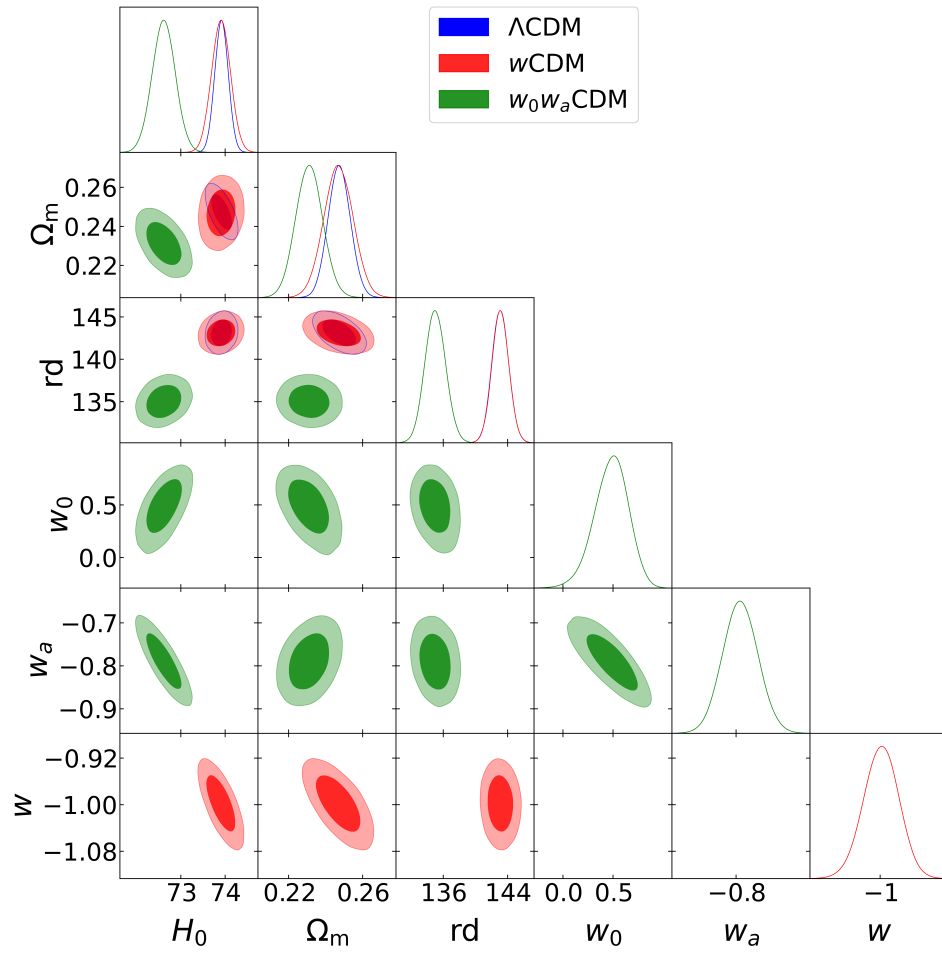
Figure 4.3: Data 3

Figure 4.4: Data 4

Figure 4.5: Data 5

Figure 4.6: Data 6

4.2 Inference

The observed result shows a trend in constraining the H_0 value. the value observed with the apparent magnitude data is lower when compared to the distance modulus data. As the distance modulus data is obtained from apparent magnitude by fixing the absolute magnitude. That is in apparent magnitude data the late time measurement alleviated the Hubble constant, which means that the so called Hubble tension is no longer existing. The OHD data and BAO data maes this result more accurate, more specificaly OHD data Helps in constraining the Hubble constant more precisely.

The same data combinations are used in three different Dark energy claiming models and the same result was observed.

4.3 conclusion

The tension was mainly triggered by the 2019 claim that the Hubble–Lemaître constant H_0, estimated from the local Cepheid–type Ia supernova (SN Ia) distance ladder, was in conflict with the value extrapolated from Cosmic Microwave Background (CMB) data under the assumption of the standard ΛCDM cosmological model. The respective values were $H_0 = 74.0 \pm 1.4 \, \mathrm{km \, s^{-1} \, Mpc^{-1}}$ and $H_0 = 67.4 \pm 0.5 \, \mathrm{km \, s^{-1} \, Mpc^{-1}}$, indicating a discrepancy at the 4.4σ level. The H_0 can be measured in 2 ways, model dependent(plank team) and model independent. the plank team used the CMB spectra for the measurement in which they had very low error bar. The model independent measurement was in late time universe using the supernovae data which was yielded by the local distance ladder method. *distance ladder method* is a stepwise approach used to measure the Hubble constant H_0, which quantifies the universe's expansion rate. It involves three key steps: first, precise geometric distances are obtained for nearby galaxies hosting Cepheid variable stars. Second, Cepheids in galaxies that also host Type Ia supernovae (SNe Ia) are used to calibrate the intrinsic brightness of these supernovae. Third, this calibration is applied to distant SNe Ia in the Hubble flow, where redshift is dominated by cosmic expansion. A simultaneous statistical fit, incorporating measurement

uncertainties and covariances, allows for a consistent and precise determination of H_0. This method forms a cornerstone of observational cosmology and enables independent cross-checks of early-universe predictions. To improve the precision of this measurement, the team expanded the sample of calibrator Type Ia supernovae (SNe Ia) from 19 to 42, observed across 37 host galaxies, systematic uncertainties in SN Ia data (SNcov), the impact of Cepheid metallicity (Zcov), and background noise from crowded star fields. Photometric errors and biases from dust extinction and crowded fields were minimized by using high-quality Hubble Space Telescope (HST) imaging in both optical and near-infrared (NIR) bands. NIR data helped reduce the impact of dust, while careful modeling of each star's environment using artificial star tests helped correct for crowding. The HST data were reprocessed with updated calibrations, including improved flat fields and distortion corrections. This significantly increased the statistical power of the analysis. The result obtained gives us a clear view that when we use the distance modulus data we get the value of H_0 between $72 - 74\mathrm{km\ s}^{-1}\mathrm{Mpc}^{-1}$ and when we take the apparent magnitude data from $65 - 67\mathrm{km\ s}^{-1}\mathrm{Mpc}^{-1}$ which means that the absolute magnitude that they have obtained using the cephaid variables are in the low redshift range. As the absolute magnitude and Hubble constant has a degeneracy and is closely related, as we fix the absolute magnitude, we naturally fix the Hubble constant. Since the distance modulus data is derived from the apparent magnitude by fixing the absolute magnitude, fixing the absolute magnitude using late-time measurements resolves the discrepancy in the Hubble constant—implying that the so-called Hubble tension effectively disappears.

4.4   Future Scope

Further combinations of observational data — particularly from quasars (QSO) and the Cosmic Microwave Background (CMB) — can be applied using both apparent magnitude measurements and distance modulus data. Incorporating these additional data sets into the analysis provides a broader cosmological context and may help reduce uncertainties in the calibration of standard candles. This, in turn, can lead to a more precise determination of the absolute mag-

nitude of sources like Type Ia supernovae or other distance indicators. The cross-validation between low-redshift (e.g., SNe Ia and Cepheids) and high-redshift (e.g., QSOs and CMB-based constraints) observations can refine the anchoring of the distance scale and improve the consistency of cosmological parameters such as the Hubble constant. Ultimately, integrating QSO and CMB data can provide stronger constraints and clearer insights into the fixing of absolute magnitude across cosmic distances.

Bibliography

[1] Kevork Abazajian, Zheng Zheng, Idit Zehavi, David H Weinberg, Joshua A Frieman, Andreas A Berlind, Michael R Blanton, Neta A Bahcall, J Brinkmann, Donald P Schneider, et al. Cosmology and the halo occupation distribution from small-scale galaxy clustering in the sloan digital sky survey. *The Astrophysical Journal*, 625(2):613, 2005.

[2] Graeme E Addison, Gary Hinshaw, and Mark Halpern. Cosmological constraints from baryon acoustic oscillations and clustering of large-scale structure. *Monthly Notices of the Royal Astronomical Society*, 436(2):1674–1683, 2013.

[3] Nikki Arendse, Adriano Agnello, and Radosław J Wojtak. Low-redshift measurement of the sound horizon through gravitational time-delays. *Astronomy & Astrophysics*, 632:A91, 2019.

[4] Daniel Baumann. *Cosmology*. Cambridge University Press, 2022.

[5] Sean M Carroll. *Spacetime and geometry*. Cambridge University Press, 2019.

[6] Marc Kamionkowski and Arthur Kosowsky. The cosmic microwave background and particle physics. *Annual Review of Nuclear and Particle Science*, 49(1):77–123, 1999.

[7] Andrew Liddle. *An introduction to modern cosmology*. John Wiley & Sons, 2015.

[8] Cong Ma and Tong-Jie Zhang. Power of observational hubble parameter data: a figure of merit exploration. *The Astrophysical Journal*, 730(2):74, 2011.

[9] Ahmad Mehrabi and Jackson Levi Said. Gaussian discriminators between λ cdm and wcdm cosmologies using expansion data. *The European Physical Journal C*, 82(9):806, 2022.

[10] Mehrdad Mirbabayi, Leonardo Senatore, Eva Silverstein, and Matias Zaldarriaga. Gravitational waves and the scale of inflation. *Physical Review D*, 91(6):063518, 2015.

[11] John A Peacock. *Cosmological physics*. Cambridge university press, 1999.

[12] Adam G Riess, Wenlong Yuan, Lucas M Macri, Dan Scolnic, Dillon Brout, Stefano Casertano, David O Jones, Yukei Murakami, Gagandeep S Anand, Louise Breuval, et al. A comprehensive measurement of the local value of the hubble constant with 1 km s- 1 mpc- 1 uncertainty from the hubble space telescope and the sh0es team. *The Astrophysical journal letters*, 934(1):L7, 2022.

[13] N Sarath, ND Jerin Mohan, and Titus K Mathew. Running vacuum cosmology with bulk viscous matter. *Modern Physics Letters A*, 38(20n21):2350099, 2023.

[14] Robert J Scherrer. Mapping the chevallier-polarski-linder parametrization onto physical dark energy models. *Physical Review D*, 92(4):043001, 2015.

[15] JK Singh, H Balhara, P Singh, et al. The constrained accelerating universe in f (r, t) gravity. *Astronomy and Computing*, 46:100795, 2024.

[16] Roberto Trotta. Bayes in the sky: Bayesian inference and model selection in cosmology. *Contemporary Physics*, 49(2):71–104, 2008.

[17] Bao Wang, Martín López-Corredoira, and Jun-Jie Wei. The hubble tension survey: A statistical analysis of the 2012–2022 measurements. *Monthly Notices of the Royal Astronomical Society*, 527(3):7692–7700, 12 2023.